PNAS
www.pnas.org

Supplementary Information for

A structural framework for unidirectional transport by a bacterial ABC exporter

Chengcheng Fan[a], Jens T. Kaiser[a], and Douglas C. Rees[a,b,1]

[a] Division of Chemistry and Chemical Engineering, California Institute of Technology, Pasadena, CA 91125

[b] Howard Hughes Medical Institute, California Institute of Technology, Pasadena, CA 91125

[1] Correspondence: Douglas C. Rees

Email: dcrees@caltech.edu

This PDF file includes:

www.pnas.org/cgi/doi/10.1073/pnas.2006526117

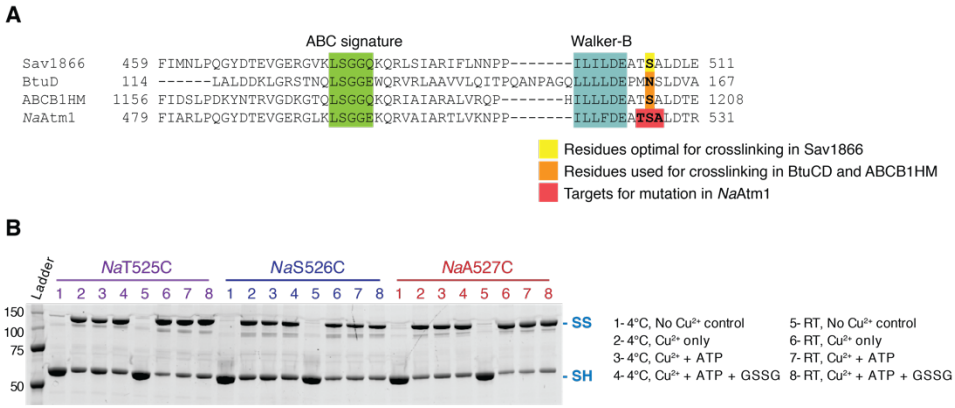

Figure S1. Screening candidate residues in *Na*Atm1 for disulfide crosslinking. (**A**) Partial sequence alignments of NBDs of various ABC transporters. (**B**) SDS-PAGE of the products of crosslinking with Cu (II)(1,10-phenanthroline)$_3$ under different conditions for the three cysteine variants in this report. RT = room temperature, SS = crosslinked species, SH = uncrosslinked (disulfide reduced) species.

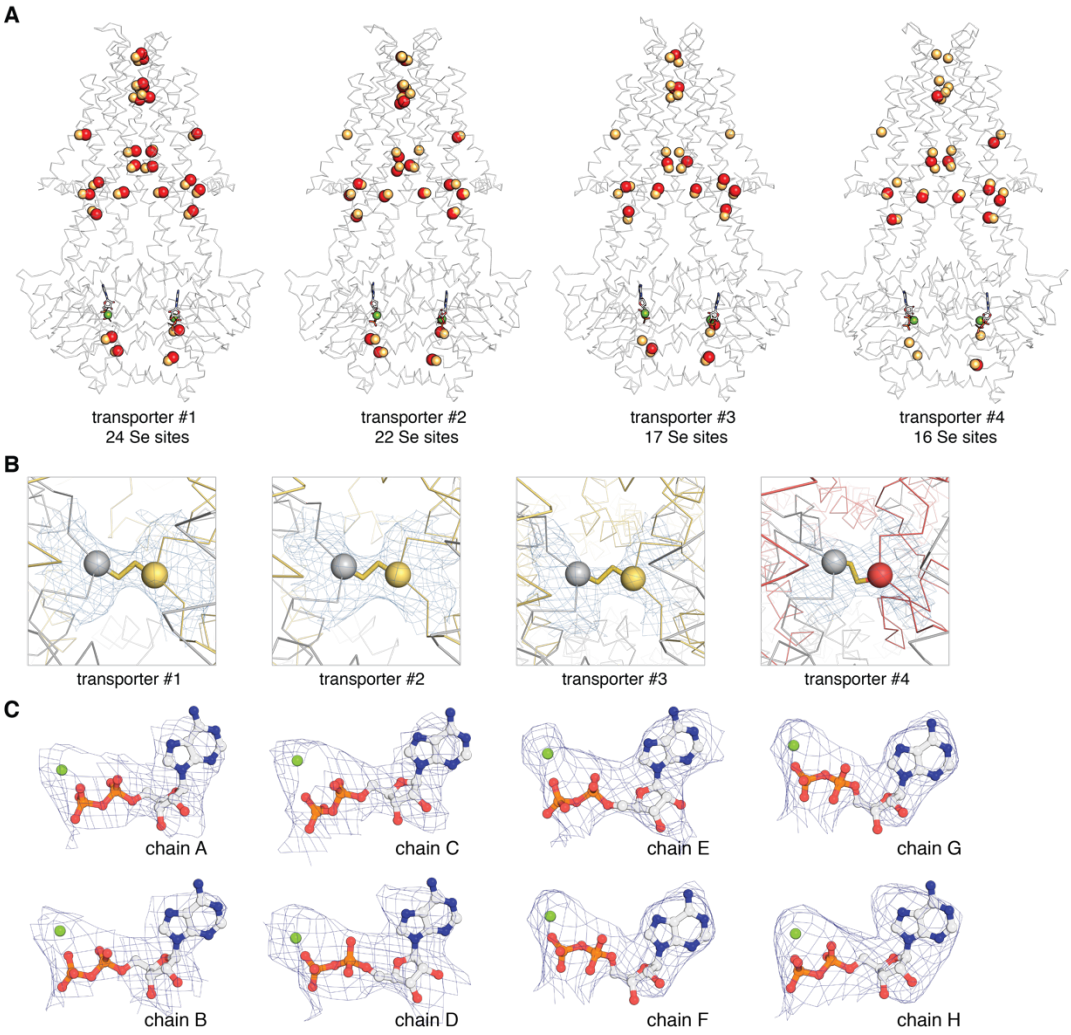

Figure S2. *Na*A527C inward-facing occluded structures. (**A**) Location of selenium sites in the four transporters present in the selenomethionine-substituted *Na*A527C asymmetric unit. The selenium sites identified in Autosol of Phenix (1) are shown in red spheres, the sulfur atoms of methionine residues from the refined model are shown in yellow spheres, and nucleotides are shown in sticks with Mg^{2+} shown in green spheres. (**B**) Disulfide bridges in the four transporters in the asymmetric unit. The Cα positions corresponding to C527 in the two chains are depicted as grey and yellow spheres for transporters #1-3, and grey and red spheres for transporter #4, separately. (**C**) Composite omit map showing the electron densities for the bound MgADP in different chains of *Na*A527C in the asymmetric unit.

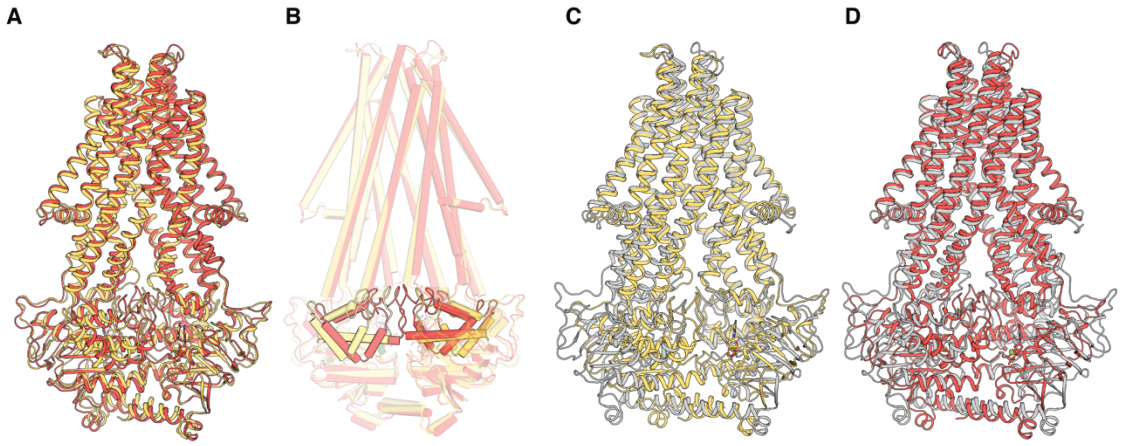

Figure S3. **Structural alignments of *Na*A527C in the inward-facing occluded conformations.** (**A**) Alignment of *Na*A527C inward-facing occluded conformation #1 (yellow) to *Na*A527C inward-facing occluded conformation #2 (red) with an overall rmsd of 1.7 Å. The relative rotation of the α-helical subdomains in the NBDs between the two states is shown in (**B**). (**C**) Alignment of *Na*A527C inward-facing occluded conformation #1 (yellow) to *Na*Atm1 inward-facing conformation (PDB ID: 4MRN) (grey) with an overall rmsd of 2.1 Å. (**D**) Alignment of *Na*A527C inward-facing occluded conformation #2 (red) to *Na*Atm1 inward-facing conformation (PDB ID: 4MRN) (grey) with an overall rmsd of 4.4 Å. Nucleotides are shown in sticks with Mg^{2+} shown as green spheres.

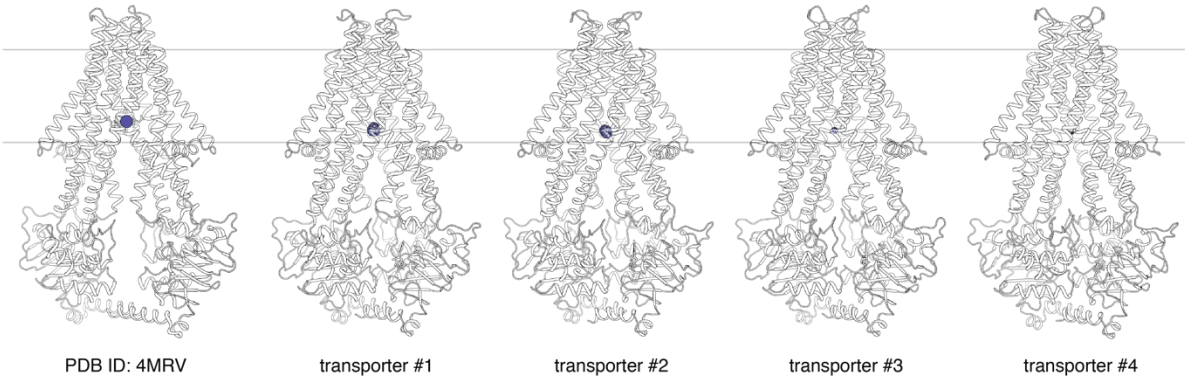

Figure S4. **Binding of GS-Hg to *Na*A527C inward-facing occluded structures.** Anomalous electron density maps calculated from data collected at the Hg edge, contoured at the 5 σ levels (dark blue) for *Na*A527C crystallized in the presence of GS-Hg. For comparison, the structure of *Na*Atm1 with GS-Hg bound (PDB ID: 4MRV) is indicated (left) with mercury shown in purple sphere. Nucleotides are shown in sticks with Mg^{2+} shown as spheres.

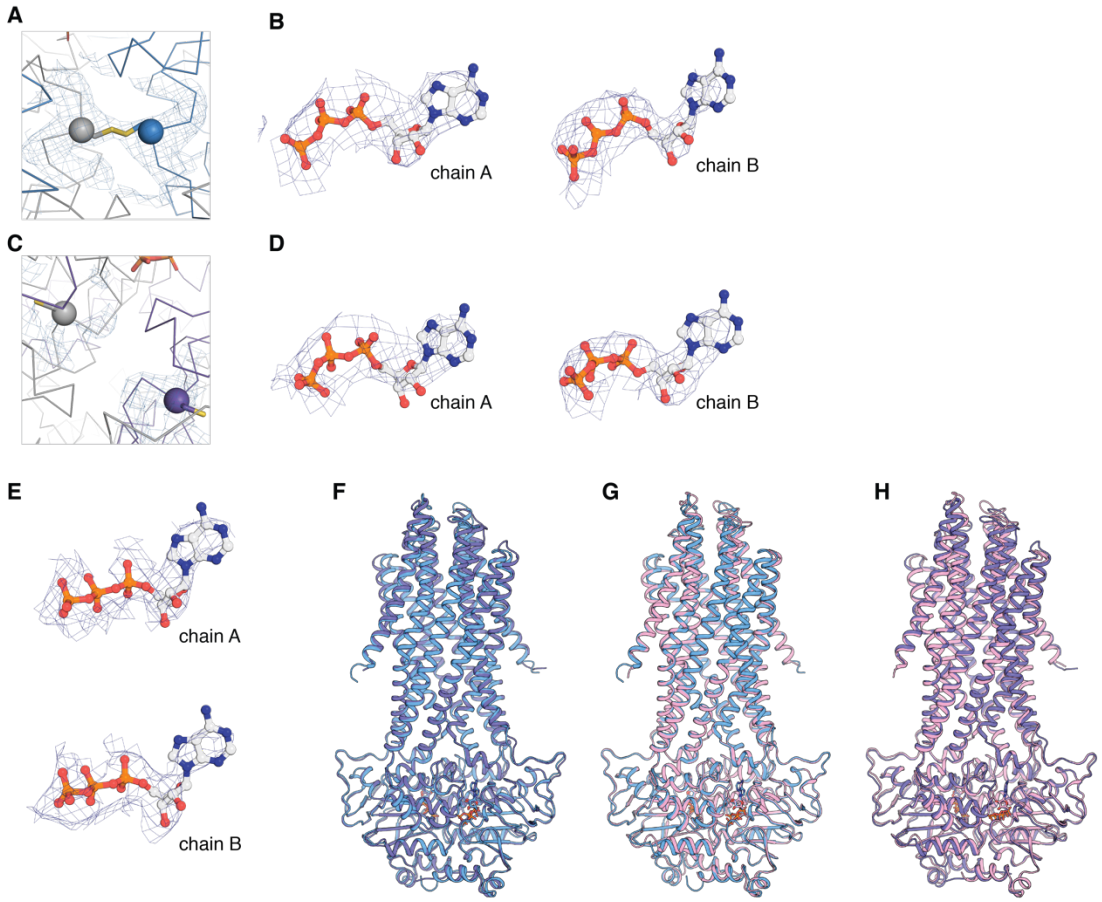

Figure S5. ***Na*Atm1 in the occluded conformations.** (**A**) Disulfide bridge formed by S526C in the *Na*S526C structure with the Cα positions shown as grey and blue spheres. (**B**) Composite omit map showing the electron densities for the bound ATP in the dimeric *Na*S526C structure. (**C**) T525C residues in the *Na*T525C occluded structure with the Cα positions shown as grey and purple spheres. (**D**) Composite omit map showing the electron densities for the bound ATP in the dimeric *Na*T525C structure. (**E**) Composite omit map showing the electron density for the bound ATP in the dimeric *Na*E523Q structure. (**F**) *Na*T525C overall structural alignment to *Na*S526C with an overall rmsd of 0.5 Å. (**G**) *Na*E523Q overall structural alignment to *Na*S526C with an overall rmsd of 0.5 Å. (**H**) *Na*E523Q overall structural alignment to *Na*T525C with an overall rmsd of 0.7 Å. In (**F-H**), *Na*S526C is colored in blue, *Na*T525C in purple, and *Na*E523Q in pink. Nucleotides are shown in sticks.

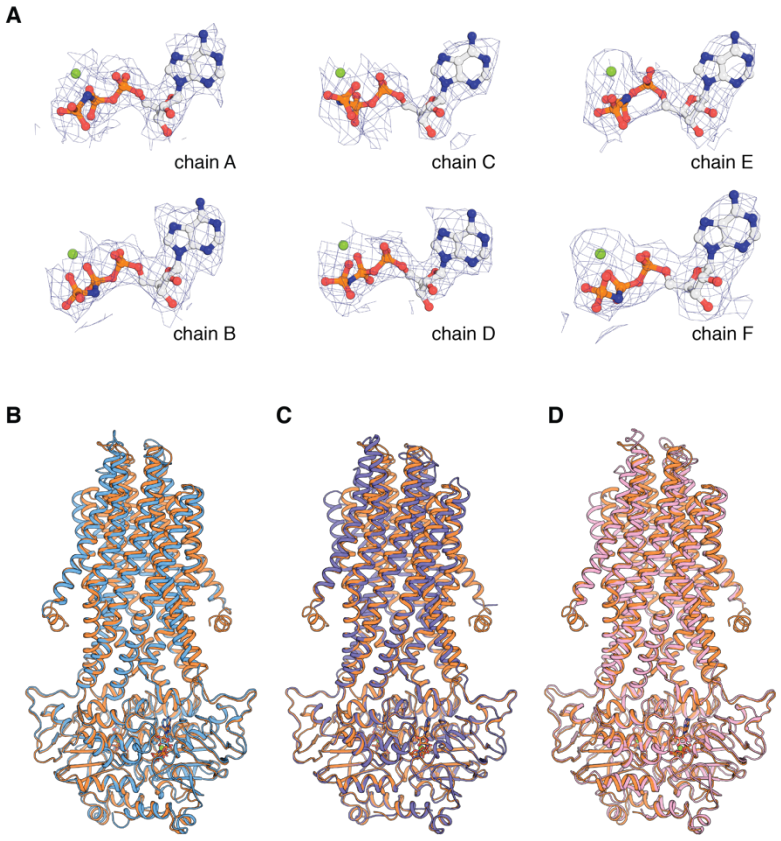

Figure S6. **Structural alignments of wild type *Na*Atm1 with MgAMPPNP in the occluded conformation.** (**A**) Composite omit map showing the electron densities for the bound MgAMPPNP in the three copies of *Na*Atm1 in the asymmetric unit. *Na*Atm1 occluded structure alignments to (**B**) *Na*S526C with an overall rmsd of 1.1 Å, (**C**) *Na*T525C with an overall rmsd of 0.9 Å, and (**D**) *Na*E523Q with an overall rmsd of 1.1 Å. In (**B-D**), *Na*Atm1 occluded structure colored in orange, *Na*S526C in blue, *Na*T525C in purple and *Na*E523Q in pink. Nucleotides are shown in sticks with Mg^{2+} shown as green spheres.

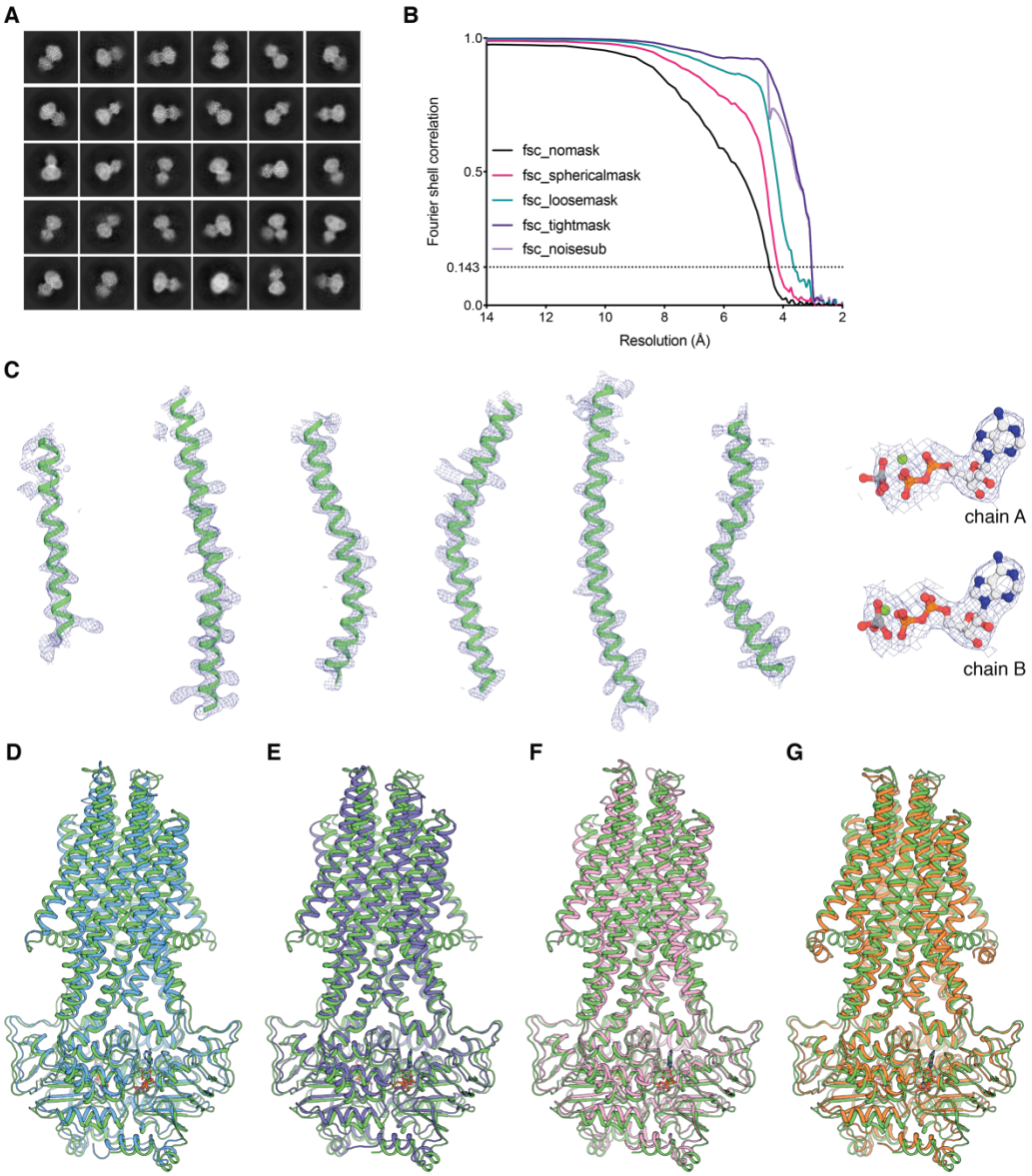

Figure S7. Single particle cryo-EM structure of *Na*Atm1 in the closed conformation stabilized with MgADPVO$_4$. (**A**) Examples of 2D classes. (**B**) Fourier shell correlation (FSC) curve showing the resolution estimate for the final reconstruction, generated from the final refinement in cryoSPARC 2 (2). (**C**) Density fitting for different TM helices and nucleotides (MgADPVO$_4$). Overall structural alignments to the occluded crystal structures of (**D**) *Na*S526C, (**E**) *Na*T525C, (**F**) *Na*E523Q and (**G**) *Na*Atm1 occluded with rmsds of 2.0 Å, 2,1 Å, 2.0 Å and 1.7 Å, respectively. In (**D-G**), the *Na*Atm1 closed structure is shown in green, *Na*S526C in blue, *Na*T525C in purple, *Na*E523Q in pink and *Na*Atm1 occluded structure is shown in orange. Nucleotides are shown as sticks and Mg^{2+} as green spheres.

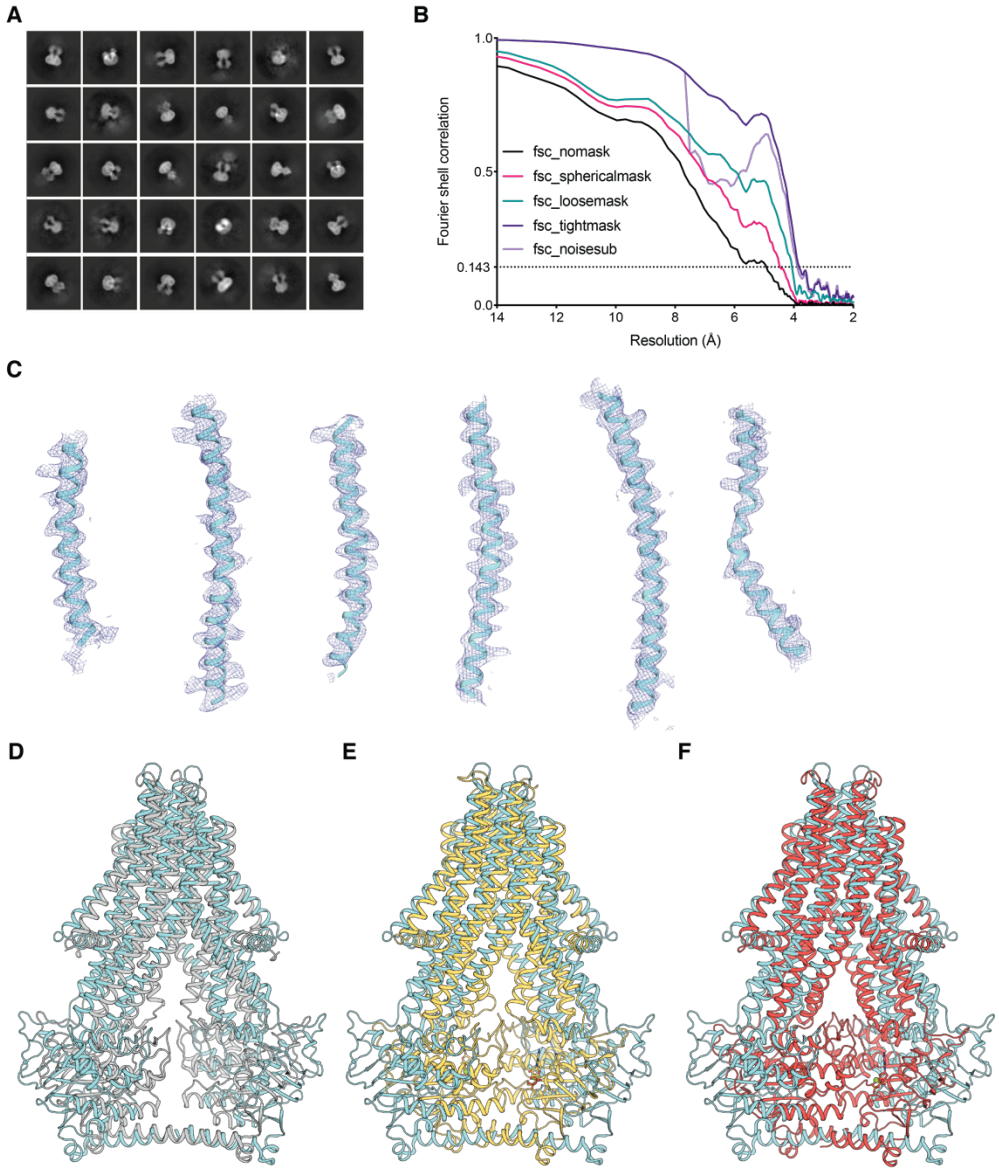

Figure S8. Single particle cryo-EM structure of *Na*Atm1 in the wide-open inward-facing conformation. (**A**) Examples of 2D classes. (**B**) FSC curve showing the resolution estimate for the final reconstruction, generated from the final refinement in cryoSPARC 2 (2). (**C**) Density fitting for different TM helices. Overall structural alignments of the wide-open inward-facing conformation (cyan) to (**D**) *Na*Atm1 inward-facing conformation (PDB ID: 4MRN) (grey), (**E**) *Na*A527C inward-facing occluded state #1 (yellow), and (**F**) *Na*A527C inward-facing occluded state #2 (red) crystal structures with rmsds of 5.8 Å, 8.9 Å, and 9.3 Å, separately.

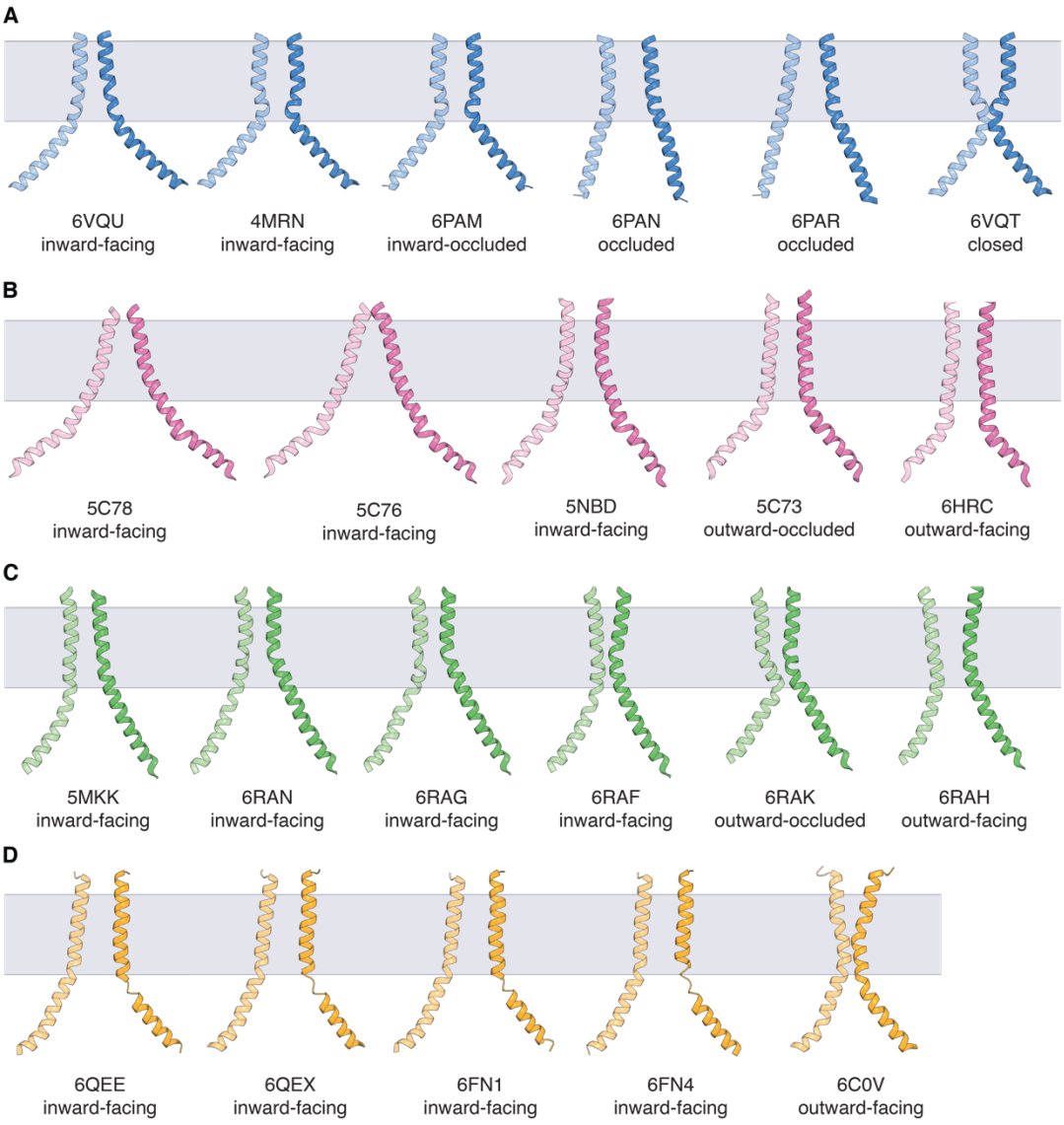

Figure S9. **TM6 comparisons for different ABC transporter systems.** (**A**) TM6 (residues 300 to 340) arrangements of representative *Na*Atm1 structures. (**B**) TM6 (residues 288 to 335) arrangements of representative PglK structures. (**C**) TM6 (residues 290 to 333 of chain A and residues 275 to 319 of chain B) arrangements of representative TmrAB structures. (**D**) TM6 (residues 324 to 370 and residues 968 to 1013) arrangements of representative ABCB1 structures. The corresponding PDB IDs and the conformational states are labeled below the structures.

Table S1. Coupling efficiencies between ATP hydrolysis and substrate translocation for ABC transporters. Coupling efficiencies for different ABC transporter systems (3-17). Coupling efficiencies are either presented in the corresponding reference or calculated based on the reported ATPase and transport activities of the transporter. Coupling efficiency = ATPase activity/transport activity.

Transporters	ATPase activity (nmol/min/mg)	Transport Activity (nmol/min/mg)	Coupling efficiency	References
ABCC3	200	1,200	0.17	Zehnpfennig et al (2009)
MalFGK	~ 1.5 - 3	~0.5 - 2	1.4 - 17	Davidson et al (1990)
OpuA	~80 - 120	~30 - 70	2	Patzlaff et al (2003)
GlnPQ	15 (min^{-1})	8.5 (min^{-1})	2	Lycklama et al (2018)
Pgp	~750 - 1,300	~500	2	Eytan et al (1996)
ABCG5/8	110	50	2.2	Wang et al (2006)
MalFGK	~1.2 - 8	~0.3 - 2	4 - 10	Dean et al (1989)
Pgp	~110	~6	18	Dong et al (1996)
HisP	580	19	31	Nikaido and Ames (1999)
ABCG2	~750	~22	34	Manolaridis et al (2018)
TmrAB	~1,100	~30	37	Hofmann et al (2019)
BtuCDF	~400	~4	100	Borths et al (2005)
***Na*Atm1**	150	1.5	100	This study
HmuUV	~130	~1.1	120	Woo et al (2012)
MalFGK	4,000	1.2	3,300	Chen et al (2001)
ABCB6	610	0.03	20,000	Chavan et al (2013)

Table S2. Raw ATPase activities of *Na*Atm1 and variants in both proteoliposomes and detergent. The ATPase activities were measured in triplicate at 10 mM MgATP and 2.5 mM GSSG at 37 °C.

Conditions	Variants				
	***Na*Atm1**	***Na*A527C**	***Na*S526C**	***Na*T525C**	***Na*E523Q**
	In proteoliposomes				
+ 10mM MgATP	51.90	1.26	55.21	13.28	1.22
	77.01	2.97	52.58	15.39	1.86
	67.60	2.93	54.32	13.43	1.00
Average	**66 ± 13**	**2 ± 1**	**54 ± 1**	**14 ± 1**	**1.4 ± 0.4**
+ 10mM MgATP + 2.5mM GSSG	118.68	7.55	69.50	20.88	-0.08
	179.94	5.66	70.29	21.00	-0.46
	157.94	6.18	68.06	20.55	0.48
Average	**152 ± 31**	**6 ± 1**	**69 ± 1**	**20.8 ± 0.2**	**0.0 ± 0.5**
	In detergent (DDM/C12E8)				
+ 10mM MgATP	122.53	11.50	108.90	57.47	5.20
	125.12	13.32	111.60	57.37	5.76
	97.76	12.30	112.40	56.94	3.30
Average	**115 ± 15**	**12.4 ± 0.9**	**111 ± 2**	**57.3 ± 0.3**	**5 ± 1**
+ 10mM MgATP + 2.5mM GSSG	215.77	14.16	104.30	42.67	3.25
	200.91	15.01	103.80	42.01	4.76
	202.41	15.10	103.20	42.88	4.26
Average	**206 ± 8**	**14.8 ± 0.5**	**103.8 ± 0.6**	**42.5 ± 0.5**	**4.1 ± 0.8**

Table S3. Raw transport activities of *Na*Atm1 and variants. The transport activities for various controls and the different *Na*Atm1 variants were measured in triplicate at 10 mM MgATP and 2.5 mM GSSG at 37 °C.

Samples	Transport rate (nmol/mg protein) at various time points (min)						Transport rates (nmole/min/mg)
	0	15	30	45	60	75	
***Na*Atm1 PLS +MgATP +GSSG**	28.17	45.49	69.95	81.08	113.06	141.67	1.488
	28.05	49.95	64.09	94.01	125.89	139.62	1.554
	26.57	54.53	77.96	83.45	114.33	149.99	1.528
Average	**27.6 ± 0.9**	**50 ± 5**	**71 ± 7**	**86 ± 7**	**118 ± 7**	**144 ± 5**	**1.52 ± 0.03**
***Na*Atm1 PLS +GSSG**	26.69	26.22	30.82	34.07	34.73	39.73	0.179
	26.08	28.78	37.44	36.06	38.74	32.31	0.1137
	26.59	30.69	36.27	35.48	31.99	38.69	0.1211
Average	**26.5 ± 0.3**	**29 ± 2**	**35 ± 4**	**35 ± 1**	**35 ± 3**	**37 ± 4**	**0.14 ± 0.04**
***Na*Atm1 PLS +MgATP**	2.84	1.03	2.95	2.98	1.13	1.48	-0.01235
	3.39	1.59	3.58	2.29	2.17	1.83	-0.01406
	3.39	2.54	4.10	2.08	1.65	-1.82	-0.05857
Average	**3.2 ± 0.3**	**1.7 ± 0.7**	**3.5 ± 0.6**	**2.5 ± 0.5**	**1.7 ± 0.5**	**0 ± 2**	**-0.03 ± 0.03**
***Na*Atm1 PLS**	3.30	1.80	3.34	2.64	1.48	1.76	-0.01782
	3.39	1.76	3.75	2.18	1.31	1.59	-0.02279
	3.39	0.16	4.03	3.30	2.04	3.95	0.01463
Average	**3.4 ± 0.1**	**1.2 ± 0.9**	**3.7 ± 0.3**	**2.7 ± 0.6**	**1.6 ± 0.4**	**2 ± 1**	**-0.01 ± 0.02**
Liposomes +GSSG	20.25	22.67	29.57	17.30	20.47	16.88	-0.06808
	14.00	21.70	25.88	18.91	16.76	16.41	-0.01854
	12.87	20.42	29.74	2.07	19.66	19.29	0.004169
Average	**16 ± 4**	**22 ± 1**	**28 ± 2**	**13 ± 9**	**19 ± 2**	**18 ± 2**	**-0.03 ± 0.04**
***Na*A527C PLS +MgATP +GSSG**	23.88	19.64	31.19	30.18	26.25	37.11	0.1618
	24.36	26.97	32.05	31.50	33.88	35.79	0.1473
	19.28	26.69	33.64	31.78	29.64	35.41	0.1669
Average	**23 ± 3**	**24 ± 4**	**32 ± 1**	**31.2 ± 0.9**	**30 ± 4**	**36.1 ± 0.9**	**0.16 ± 0.01**
***Na*S526C PLS +MgATP +GSSG**	22.86	42.06	53.21	66.26	77.55	79.59	0.7679
	21.26	41.68	59.75	61.69	84.84	92.92	0.9328
	22.58	37.91	61.09	64.64	82.63	103.12	1.029
Average	**22.2 ± 0.9**	**41 ± 2**	**58 ± 4**	**64 ± 2**	**82 ± 4**	**92 ± 12**	**0.9 ± 0.1**
***Na*T525C PLS +MgATP +GSSG**	23.32	25.75	15.61	49.92	58.39	63.36	0.6332
	20.60	26.69	40.53	51.72	52.88	37.39	0.3309
	21.82	25.94	39.12	42.16	59.62	57.18	0.535
Average	**22 ± 1**	**26.1 ± 0.5**	**32 ± 14**	**48 ± 5**	**57 ± 4**	**53 ± 14**	**0.5 ± 0.2**
***Na*E523Q PLS +MgATP +GSSG**	21.82	26.31	30.16	31.69	32.19	32.12	0.1345
	16.01	24.62	30.91	8.99	35.00	33.71	0.1862
	17.88	21.80	23.30	32.07	35.00	34.47	0.2501
Average	**19 ± 3**	**24 ± 2**	**28 ± 4**	**24 ± 13**	**34 ± 2**	**33 ± 1**	**0.19 ± 0.06**

Table S4. Data collection and refinement statistics of *Na*A527C.

	***Na*A527C native**	***Na*A527C SeMet**
Beamline	SSRL 12-2	SSRL 12-2
Wavelength (Å)	0.97946	0.97949
Resolution range (Å)	39.37 - 3.70 (3.832 - 3.70)	39.72 - 4.50 (4.66 - 4.50)
Space group	P 1	P 1
Unit cell (Å, °)	129.18 133.61 134.26 110.619 98.282 101.2	129.19 133.14 134.27 109.61 98.51 101.67
Total reflections	603652 (61595)	972530 (99987)
Unique reflections	84628 (7646)	47277 (4667)
Multiplicity	7.1 (7.3)	20.6 (21.4)
Completeness (%)	97.55 (89.28)	99.3 (99.3)
Mean I/sigma(I)	7.31 (0.74)	8.1 (1.4)
Wilson B-factor	141.79	163.64
R-merge	0.167 (3.050)	0.291 (3.241)
R-meas	0.180 (3.283)	0.298 (3.320)
R-pim	0.067 (1.206)	0.066 (0.712)
CC1/2	0.999 (0.412)	0.998 (0.761)
CC*	1.000 (0.764)	
Reflections used in refinement	83473 (7643)	
Reflections used for R-free	4185 (346)	
R-work	0.240 (0.356)	
R-free	0.288 (0.400)	
CC(work)	0.787 (0.709)	
CC(free)	0.841 (0.703)	
Number of non-hydrogen atoms	36839	
macromolecules	36615	
ligands	224	
Protein residues	4722	
RMS (bonds) (Å)	0.004	
RMS (angles) (°)	0.95	
Ramachandran favored (%)	97.95	
Ramachandran allowed (%)	1.96	
Ramachandran outliers (%)	0.09	
Rotamer outliers (%)	0.40	
Clashscore	6.13	
Average B-factor	178.14	
macromolecules	178.04	
ligands	194.08	

**Statistics for the highest-resolution shell are shown in parentheses.

Table S5. Data collection and refinement statistics of *Na*S526C.

	***Na*S526C SeMet**
Beamline	SSRL 12-2
Wavelength (Å)	0.97938
Resolution range (Å)	39.71 - 3.40 (3.522 - 3.40)
Space group	P 21 21 21
Unit cell (Å, °)	95.5 134.58 190.12 90 90 90
Total reflections	916579 (84633)
Unique reflections	34343 (3016)
Multiplicity	26.7 (25.1)
Completeness (%)	98.64 (89.27)
Mean I/sigma(I)	17.26 (1.19)
Wilson B-factor	138.15
R-merge	0.148 (3.919)
R-meas	0.151 (4.000)
R-pim	0.029 (0.792)
CC1/2	1.000 (0.588)
CC*	1.000 (0.861)
Reflections used in refinement	33962 (3012)
Reflections used for R-free	1696 (153)
R-work	0.192 (0.295)
R-free	0.234 (0.377)
CC(work)	0.727 (0.820)
CC(free)	0.865 (0.750)
Number of non-hydrogen atoms	8921
macromolecules	8859
ligands	62
Protein residues	1147
RMS (bonds) (Å)	0.002
RMS (angles) (°)	0.57
Ramachandran favored (%)	98.77
Ramachandran allowed (%)	1.23
Ramachandran outliers (%)	0.00
Rotamer outliers (%)	0.88
Clashscore	7.07
Average B-factor	196.93
macromolecules	196.93
ligands	197.86

**Statistics for the highest-resolution shell are shown in parentheses.

Table S6. Data collection and refinement statistics of *Na*T525C.

	*Na*T525C native	*Na*T525C SeMet
Beamline	APS GM/CA 23-IDB	APS GM/CA 23-IDB
Wavelength (Å)	1.033202	0.979338
Resolution range (Å)	39.1 - 3.65 (3.78 - 3.65)	39.31 - 3.90 (4.21 - 3.90)
Space group	P 21 21 21	P 21 21 21
Unit cell (Å, °)	94.164 135.415 191.592 90 90 90	93.78 136.37 192.48 90 90 90
Total reflections	246061 (22321)	237126 (49769)
Unique reflections	27912 (2712)	23170 (4675)
Multiplicity	8.8 (8.1)	10.2 (10.6)
Completeness (%)	97.77 (97.54)	99.9 (99.9)
Mean I/sigma(I)	14.33 (1.11)	12.1 (1.6)
Wilson B-factor	172.32	180.32
R-merge	0.076 (2.002)	0.100 (1.852)
R-meas	0.080 (2.146)	0.106 (1.945)
R-pim	0.027 (0.758)	0.033 (0.590)
CC1/2	0.999 (0.634)	1.000 (0.586)
CC*	1.000 (0.881)	
Reflections used in refinement	27348 (2699)	
Reflections used for R-free	1356 (126)	
R-work	0.251 (0.430)	
R-free	0.285 (0.475)	
CC(work)	0.713 (0.364)	
CC(free)	0.877 (0.304)	
Number of non-hydrogen atoms	8835	
macromolecules	8773	
ligands	62	
Protein residues	1135	
RMS (bonds) (Å)	0.003	
RMS (angles) (°)	0.63	
Ramachandran favored (%)	97.70	
Ramachandran allowed (%)	2.30	
Ramachandran outliers (%)	0.00	
Rotamer outliers (%)	0.22	
Clashscore	7.07	
Average B-factor	214.38	
macromolecules	214.56	
ligands	189.06	

**Statistics for the highest-resolution shell are shown in parentheses.

Table S7. Data collection and refinement statistics of *Na*E523Q.

	***Na*E523Q SeMet**
Beamline	SSRL 12-2
Wavelength (Å)	0.97946
Resolution range (Å)	38.63 - 3.30 (3.419 - 3.30)
Space group	P 21 21 21
Unit cell (Å, °)	89.346 115.354 184.536 90 90 90
Total reflections	387847 (39220)
Unique reflections	29277 (2861)
Multiplicity	13.2 (13.6)
Completeness (%)	99.32 (98.72)
Mean I/sigma(I)	11.11 (1.01)
Wilson B-factor	103.58
R-merge	0.190 (2.680)
R-meas	0.200 (2.784)
R-pim	0.054 (0.748)
CC1/2	1.000 (0.700)
CC*	1.000 (0.908)
Reflections used in refinement	29179 (2845)
Reflections used for R-free	1434 (127)
R-work	0.234 (0.330)
R-free	0.300 (0.439)
CC(work)	0.684 (0.848)
CC(free)	0.827 (0.615)
Number of non-hydrogen atoms	8842
macromolecules	8780
ligands	62
Protein residues	1136
RMS (bonds) (Å)	0.002
RMS (angles) (°)	0.63
Ramachandran favored (%)	97.52
Ramachandran allowed (%)	2.48
Ramachandran outliers (%)	0.00
Rotamer outliers (%)	1.77
Clashscore	8.24
Average B-factor	134.03
macromolecules	133.82
ligands	163.57

**Statistics for the highest-resolution shell are shown in parentheses.

Table S8. Data collection and refinement statistics of *Na*Atm1.

	*Na*Atm1 native	*Na*Atm1 SeMet
Beamline	SSRL 12-2	SSRL 12-2
Wavelength (Å)	0.97946	0.9793
Resolution range (Å)	39.33 - 3.35 (3.47 - 3.35)	39.85 - 3.60 (3.67 - 3.60)
Space group	P 21	P 21
Unit cell (Å, °)	169.648 92.498 237.691 90 110.34 90	170.10 92.21 237.47 90 110.58 90
Total reflections	686114 (60885)	559063 (30390)
Unique reflections	98507 (9041)	79094 (4376)
Multiplicity	7.0 (6.4)	7.1 (6.9)
Completeness (%)	97.85 (91.11)	98.1 (95.8)
Mean I/sigma(I)	9.43 (0.97)	7.5 (1.1)
Wilson B-factor	91.20	94.99
R-merge	0.174 (1.768)	0.211 (1.942)
R-meas	0.189 (1.927)	0.228 (2.100)
R-pim	0.071 (0.754)	0.086 (0.787)
CC1/2	0.999 (0.530)	0.994 (0.466)
CC*	1.000 (0.832)	
Reflections used in refinement	97914 (9035)	
Reflections used for R-free	4897 (425)	
R-work	0.254 (0.353)	
R-free	0.282 (0.365)	
CC(work)	0.740 (0.685)	
CC(free)	0.529 (0.606)	
Number of non-hydrogen atoms	26975	
macromolecules	26783	
ligands	192	
Protein residues	3464	
RMS (bonds) (Å)	0.003	
RMS (angles) (°)	0.60	
Ramachandran favored (%)	97.35	
Ramachandran allowed (%)	2.59	
Ramachandran outliers (%)	0.06	
Rotamer outliers (%)	0.58	
Clashscore	8.33	
Average B-factor	120.02	
macromolecules	120.15	
ligands	101.67	

**Statistics for the highest-resolution shell are shown in parentheses.

Table S9. Cryo-EM data collection, refinement and validation statistics

	Closed	Inward-facing
Data Collection and processing		
Microscope	Titan Krios at S2C2	Titan Krios at Caltech Cryo-EM facility
Camera	Gatan K3	Gatan K2 Summit
Magnification	x29,000	x165,000
Voltage (keV)	300	300
Exposure (e/Å^2)	48.6	36
Pixel size (Å)	0.852	0.834
Defocus Range (μm)	- 1.7 to -2.4	- 1.0 to -3.5
Initial Particle Image (no.)	3,978,816	1,145,444
Final Particle Image (no.)	169,278	102,076
Symmetry Imposed	C2	C2
Map Resolution (Å)	3.03	3.88
FSC Threshold	0.143	0.143
Map Resolution Range (Å)	2.8-3.8	3.8 - 4.5
Refinement		
Initial Model Used	PDB ID: 6PAR	PDB ID: 4MRN
Model Resolution (Å)	3.0	3.9
FSC Threshold	0.143	0.143
Map Sharpening B-factor (Å^2)	-86	-121
Model composition		
non-hydrogen atoms	9144	9156
protein residues	1168	1178
ligands	ADP: 2; MG: 2; VO4:2	-
Average B-factors (Å^2)		
protein	94.1	22.5
ligands	86.7	-
R.m.s. deviations		
Bond length (Å)	0.005	0.007
Bond angles (°)	0.967	0.929
Validation		
MolProbity score	2.2	1.67
Clashscore	10.2	5.1
Rotamer outliers	4.9	1.7
Ramachandran plot		
Ramachandran favored (%)	97.3	96.6
Ramachandran allowed (%)	2.7	3.4
Ramachandran outliers (%)	0	0

SI References

1. P. D. Adams *et al.*, PHENIX: a comprehensive Python-based system for macromolecular structure solution. *Acta Crystallogr. D Biol. Crystallogr.* **66**, 213-221 (2010).
2. A. Punjani, J. L. Rubinstein, D. J. Fleet, M. A. Brubaker, cryoSPARC: algorithms for rapid unsupervised cryo-EM structure determination. *Nature methods* **14**, 290-296 (2017).
3. B. Zehnpfennig, I. L. Urbatsch, H. J. Galla, Functional reconstitution of human ABCC3 into proteoliposomes reveals a transport mechanism with positive cooperativity. *Biochemistry* **48**, 4423-4430 (2009).
4. A. L. Davidson, H. Nikaido, Overproduction, solubilization, and reconstitution of the maltose transport system from *Escherichia coli*. *Journal of Biological Chemistry* **265**, 4254-4260 (1990).
5. J. S. Patzlaff, T. van der Heide, B. Poolman, The ATP/substrate stoichiometry of the ATP-binding cassette (ABC) transporter OpuA. *Journal of Biological Chemistry* **278**, 29546-29551 (2003).
6. A. N. J. A. Lycklama, R. Vietrov, G. K. Schuurman-Wolters, B. Poolman, Energy Coupling Efficiency in the Type I ABC Transporter GlnPQ. *Journal of Molecular Biology* **430**, 853-866 (2018).
7. G. D. Eytan, R. Regev, Y. G. Assaraf, Functional reconstitution of P-glycoprotein reveals an apparent near stoichiometric drug transport to ATP hydrolysis. *Journal of Biological Chemistry* **271**, 3172-3178 (1996).
8. J. Wang *et al.*, Sterol transfer by ABCG5 and ABCG8: in vitro assay and reconstitution. *Journal of Biological Chemistry* **281**, 27894-27904 (2006).
9. D. A. Dean, A. L. Davidson, H. Nikaido, Maltose transport in membrane vesicles of Escherichia coli is linked to ATP hydrolysis. *Proc. Natl. Acad. Sci. U. S. A.* **86**, 9134-9138 (1989).
10. M. Dong, F. Penin, L. G. Baggetto, Efficient purification and reconstitution of P-glycoprotein for functional and structural studies. *Journal of Biological Chemistry* **271**, 28875-28883 (1996).
11. K. Nikaido, G. F. Ames, One intact ATP-binding subunit is sufficient to support ATP hydrolysis and translocation in an ABC transporter, the histidine permease. *Journal of Biological Chemistry* **274**, 26727-26735 (1999).
12. I. Manolaridis *et al.*, Cryo-EM structures of a human ABCG2 mutant trapped in ATP-bound and substrate-bound states. *Nature* **563**, 426-430 (2018).
13. S. Hofmann *et al.*, Conformation space of a heterodimeric ABC exporter under turnover conditions. *Nature* **571**, 580-583 (2019).
14. E. L. Borths, B. Poolman, R. N. Hvorup, K. P. Locher, D. C. Rees, In vitro functional characterization of BtuCD-F, the *Escherichia coli* ABC transporter for vitamin B12 uptake. *Biochemistry* **44**, 16301-16309 (2005).
15. J. S. Woo, A. Zeltina, B. A. Goetz, K. P. Locher, X-ray structure of the *Yersinia pestis* heme transporter HmuUV. *Nature structural & molecular biology* **19**, 1310-1315 (2012).
16. J. Chen, S. Sharma, F. A. Quiocho, A. L. Davidson, Trapping the transition state of an ATP-binding cassette transporter: evidence for a concerted mechanism of maltose transport. *Proc. Natl. Acad. Sci. U. S. A.* **98**, 1525-1530 (2001).
17. H. Chavan, M. M. Khan, G. Tegos, P. Krishnamurthy, Efficient purification and reconstitution of ATP binding cassette transporter B6 (ABCB6) for functional and structural studies. *Journal of Biological Chemistry* **288**, 22658-22669 (2013).